Bioresource Technology Reports 19 (2022) 101139

Contents lists available at ScienceDirect

Bioresource Technology Reports

journal homepage: www.sciencedirect.com/journal/bioresource-technology-reports

Investigation of light crude oil removal using biocoal from torrefaction of biomass waste

Berna Kekik, Halime Yakışık, Uğur Özveren *

Marmara University, Chemical Engineering Department, 34730 Goztepe, Istanbul, Turkey

ARTICLE INFO

Keywords:
Torrefaction
Biocoal
Cypress cone waste
Oil spill
Adsorption
Remediation

ABSTRACT

Oil spills pose a significant threat to aquatic life worldwide. However, cleaning up oil spills can be difficult and expensive. Therefore, research on efficient and environmentally friendly methods to treat oil spills is an important issue. In this study, biocoal obtained from torrefaction of cypress cone waste at 300 °C was used to investigate the efficient and environmentally friendly methods for treating oil spills. In addition, RAMAN, XRD, SEM and FT-IR were used to study the morphology and structure of the biocoal-based adsorbent. Structural and morphological analyzes show that the torrefied cypress cone has a porous and heterogeneous surface, which is advantageous for adsorption of oil contaminants from seawater. The adsorption process was also evaluated by kinetic analysis. The results showed that cypress cone-based biocoal can be used as a promising adsorbent for the treatment of oil spills with a good adsorption capacity of 6.587 g/g within 120 min.

1. Introduction

Oil spills in marine and coastal waters from transportation, application, extraction, and storage are expected to increase as the world becomes more reliant on oil. They are often the result of accidents such as collisions with oil tankers, explosions/fires, pipeline and storage tank failures during large-scale offshore oil production and transportation over long distances (Bada and Olarinre, 2012). Moreover, such accidental oil spills cause environmental disasters that affect all aspects of marine ecosystems. Therefore, environmental problems caused by oil spills are considered as one of the global challenges that science should focus on (Chen et al., 2019). Therefore, the removal of oil spills is difficult due to the complex nature of these organic sites. The choice of the outstanding treatment method for cleaning up crude oil depends on the type of crude oil spill (heavy or light) and the site. Oil spill cleanup techniques generally rely on biological, physical, and chemical methods such as mechanical pickup, dispersants, and biodegradation. Although mechanical methods are widely used, they incur higher operating costs due to the specialized equipment required. On the other hand, biological methods have some limitations as a single class of microorganisms may not effectively degrade all organic components of the oil spill (Goi et al., 2006).

Nevertheless, the adsorption process, in which the oil components are adsorbed by the adsorbents, is of great interest for economic and environmental reasons compared to the other methods of treating oil spills (Doshi et al., 2018). The most critical step in the adsorption process is the selection of the ideal adsorbent with excellent performance, environmental friendliness, low toxicity, and large surface area that can be produced at an affordable cost for commercial scale. So far, many different natural and synthetic adsorbents have been used for oil spill adsorption, such as zeolites, activated carbon, organic clays, hollow carbon fibers, straw and chitosan. In the last decade, carbonaceous materials have been widely preferred as environmentally friendly oil adsorbents because they are abundant in nature, practical, simple, inexpensive, and have better physicochemical properties compared to other natural adsorbents (Gao et al., 2017). Biocoal can be proposed as a useful pyrogenic carbonaceous adsorbent for oil adsorption, usually produced by torrefaction of plant and animal biomass under pyrolytic atmosphere. Torrefaction is a pretreatment process for biocoal production that takes place under an oxygen-free atmosphere at relatively low temperatures (usually between 200 °C and 300 °C) and increases the atomic C/H and C/O ratios (Kartal and Özveren, 2022).

In recent years, biocoal has received much attention as an adsorbent due to its numerous inherent advantages such as mesoporous structure, high porosity, exceptional aromaticity, and diverse functional surface sites (CO, OH, COOH, et al.) (Chen et al., 2021; Gurav et al., 2021; Kartal and Özveren, 2022). In addition, the removal of polar functional sites from the biomass surface by the heating effect of torrefaction increases

* Corresponding author.
E-mail address: ugur.ozveren@marmara.edu.tr (U. Özveren).

https://doi.org/10.1016/j.biteb.2022.101139
Received 19 February 2022; Received in revised form 18 June 2022; Accepted 22 June 2022
Available online 27 June 2022

the surface area available for interaction. The porous structure and heterogeneous surface chemistry have a strong impact on their adsorption potential (Lin et al., 2018). For this reason, biocoal is widely used for soil improvement, wastewater recovery, carbon capturing, and composting of organic solid waste, etc. (Nobre et al., 2016; Wang and Wang, 2019).

The surface of biocoal (π-acceptor) creates accessible adsorption sites for oil pollutants through hydrophobic interactions (Nguyen et al., 2016). Oil-based organic contaminants are readily entrapped in the porous structure of biocoal when it comes into contact with oily water, resulting in a high capacity for oil adsorption (Kandanelli et al., 2018). On the other hand, not all pores of biocoal can be considered as possible adsorption sites for petroleum-based organic contaminants because they contain larger organic compounds with a high number of carbon atoms. Crude oil contains a variety of hydrocarbons ranging from very light oil to heavy oil in amounts from 50 to 98 %. Therefore, a detailed study of the adsorption mechanism of biocoal in the treatment of crude oil contaminants from seawater is needed.

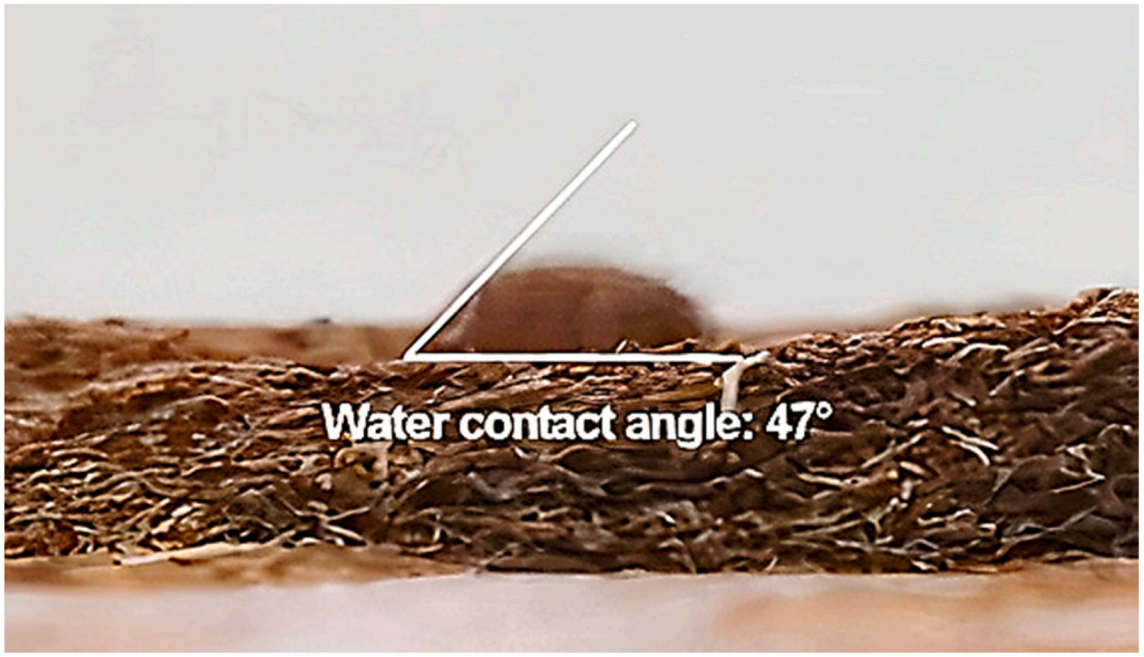

(a)

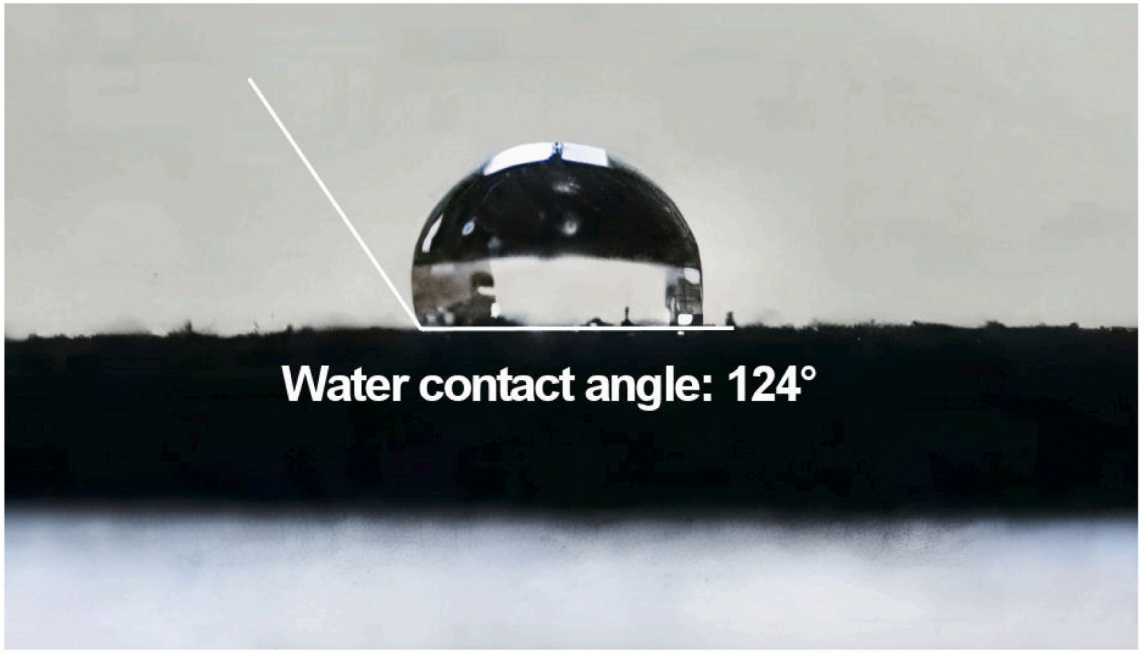

(b)

Fig. 1. Water droplet over (a) raw cypress cone (b) torrefied cypress cone.

However, there is a research gap in the application of biocoal as an adsorbent for the petroleum environment, as the capacity of biocoal has been poorly evaluated compared to other adsorbents. Therefore, the aim of this study is to fill this research gap by experimentally investigating cypress cone-based biocoal (torrefied cypress cones), which have shown great capacity to adsorb crude oil.

This study presents the synthesis and characterization of a new adsorbent from cypress cone waste for the removal of spilled crude oil. Cypress cones were preferred because they are self-growing, abundant in Turkey, and have never been studied as a biocoal precursor for crude oil treatment. To the best of our knowledge, this is the first study to investigate the efficacy of the biocoal adsorbent prepared from cypress cones in removing light crude oil and the structural and morphological properties of the torrefied cypress cones. The developed adsorbent material was analyzed using Raman, SEM, XRD, FT-IR characterization techniques. In addition, the effects of adsorption time and adsorbent amount on the performance of the biocoal adsorbent in removing light crude oil from Basra were investigated. Kinetic modeling studies were also conducted to better interpret the adsorption processes and determine whether the process was chemical or physical.

2. Materials and methods

2.1. Green synthesis of biocoal from cypress cones using torrefaction

Biocoal adsorbent is prepared by torrefaction of cypress cones in an oxygen-free environment. Samples of cypress cones were collected after ripening on the campus of Marmara University. To remove impurities, the collected cypress cones were cleaned with distilled water and dried at 25 °C for 24 h. The dry cypress cones were crushed by cutting and then ground as a biocoal feedstock. The ground cypress cone was sieved to a particle size of <315 μm. The optimal temperature for torrefaction was determined using the three component technique (Yang et al., 2007). The temperature at which the least lignin mass loss occurs and the most carbonization appears was determined in this study using TGA analysis according to the three component technique and models, including the artificial intelligence approach created by Kartal and Özveren (2021, 2022). Therefore, the sieved material was placed above the plate in the muffle furnace and heated from 25 °C to the torrefaction temperature (300 ± 5.0 °C) at a flow rate of 300 mL min^{-1} nitrogen gas. To protect the stability of the functional sites in the structure, the torrefied cypress cone was held at 300 °C for 90 min. The biocoal samples obtained from the cypress cones were stored in a climate-controlled room at 25 °C for use in subsequent adsorption studies.

2.2. Materials characterization

2.2.1. X-ray diffraction

The biocoal samples of cypress cone powder as adsorbent were placed on the recording slit of an X-ray diffractometer (Lab-X XRD-6100 Shimadzu) and irradiated with copper radiation (Cu-Kα X-rays of wavelength (λ) = 1.5406 Å). The diffraction pattern was recorded at room temperature in the 2-Theta range from 10 to 60° (with a resolution of 0.02° and a scanning speed of 2.0000 (deg/min)).

2.2.2. Raman spectroscopy

Raman spectral analysis was performed using DongWoo Optron's STEX-100 (with a 532-nm laser as the excitation source), which is equipped with an aberration-corrected high-throughput spectrograph and a CCD detector with a 0.2-nm pixel array. An optical grating dispersed the Raman scattered light captured by a TE cooled high performance CCD camera. The power of the laser beam was adjusted from 0.1 % to 100 % of the source power. Powder samples were poured onto plastic plates and then placed on the microscope's sample holder. With a white light source exposing the sample, the microscope was set to continuous scan mode with a 20-second timer for data exposure.

2.2.3. Fourier transform infrared (FT-IR) spectroscopy

The changes in functional groups on the surface of the torrefied cypress cone were observed by Fourier-transformed infrared spectroscopy (FT-IR). The spectra were recorded using an FT-IR spectrometer model FT/IR −4700 type A in the range 400–4000 cm^{-1} with a spectral resolution of 4 cm^{-1}. The potassium bromide (KBr) pellets of the torrefied cypress cone sample were prepared by mixing KBr powder with torrefied samples. The recorded background from a scan with pure KBr was automatically removed from the sample spectra.

2.2.4. Scanning electron microscopy (SEM)

A scanning electron microscopy (SEM) (ZEISS EVO MA1O0) was used to assess the morphology of the surface of torrefied cypress cones. Double-sided conductive adhesive tapes were coated with gold to prepare the samples. The SEM image was acquired at a voltage of 10 kV and a magnification of 2000×.

2.3. Adsorption kinetics

The adsorption of crude oil on torrefied cypress cones was investigated with kinetic studies using a pseudo-second-order kinetic model. Adsorption studies were performed in batches by adding 0.01 ± 0.005 g of crude oil to 100 mL seawater and incubating at 20 °C. To understand the agreement of the experimental results with the calculated results, the models were validated using the obtained regression coefficients (R^2).

3. Results

3.1. Characterization of adsorbents

The porosity of the cypress cone biomass and the diversity of reactive functional adsorption sites on the adsorbent surface are important factors in determining the oil adsorption capacity of the biomass. In this regard, information on the functional groups on the surface of the torrefied cypress cone provides a better understanding of the oil adsorption capacity of the material. Cypress cones are composed of lignin (>40 %), indicating the possibility of obtaining a high quality biocoal with excellent microporosity and suitable surface area (Suhas, 2007).

The visual hydrophobicity of the sample of the raw cypress cone and the torrefied cypress cone was tested by applying a drop of water to the surface of the raw cypress cone and the torrefied cypress cone, as shown in Fig. 1.

The contact angle of the torrefied cypress cone was drastically increased to 124° after torrefaction, compared to the raw cypress cone which was 47°. Biocoal adsorbents from torrefaction of cypress cones with a contact angle >90° are considered to be more hydrophobic. While water droplets penetrated the sample of raw cypress cone biomass, water was able to remain on the surface of the torrefied cypress cone without penetrating, which was due to its intrinsic hydrophobicity.

The FT-IR spectra of the biocoal torrefied at 300 °C resulted in torrefaction at lower temperatures leading to dehydration, incipient bond breaks and transformation products. Several peaks were examined in the graph, including a well-defined peak at 2935 cm^{-1} related to the symmetric stretching vibrations of the aliphatic bands - CH, $-CH_2$, and $-CH_3$. The location of these functional groups on the surface of torrefied cypress cones indicates that they possess high hydrophobicity and oleophilicity (Oliveira et al., 2020). The other peak observed at 1589 cm^{-1} is attributed to carboxylate groups. The region between 1500 and 1800 cm^{-1} was defined as the carbonyl and double bond region (Min et al., 2004). The hydrophobicity of fatty acids increases due to the formation of double bonds formed by the stretching of the carbonyl group (Navarathna et al., 2020). The peak at 1051 cm^{-1} is associated with cyclohexane ring vibrations. The O—H stretching of hydroxyl groups with hydrogen bending is attributed to a wide range in the 3000–3500 cm^{-1} region (Belhamdi et al., 2019). In torrefied cypress cones, the absence of a significant peak at 3300–3400 cm^{-1} for a single bond stretching of

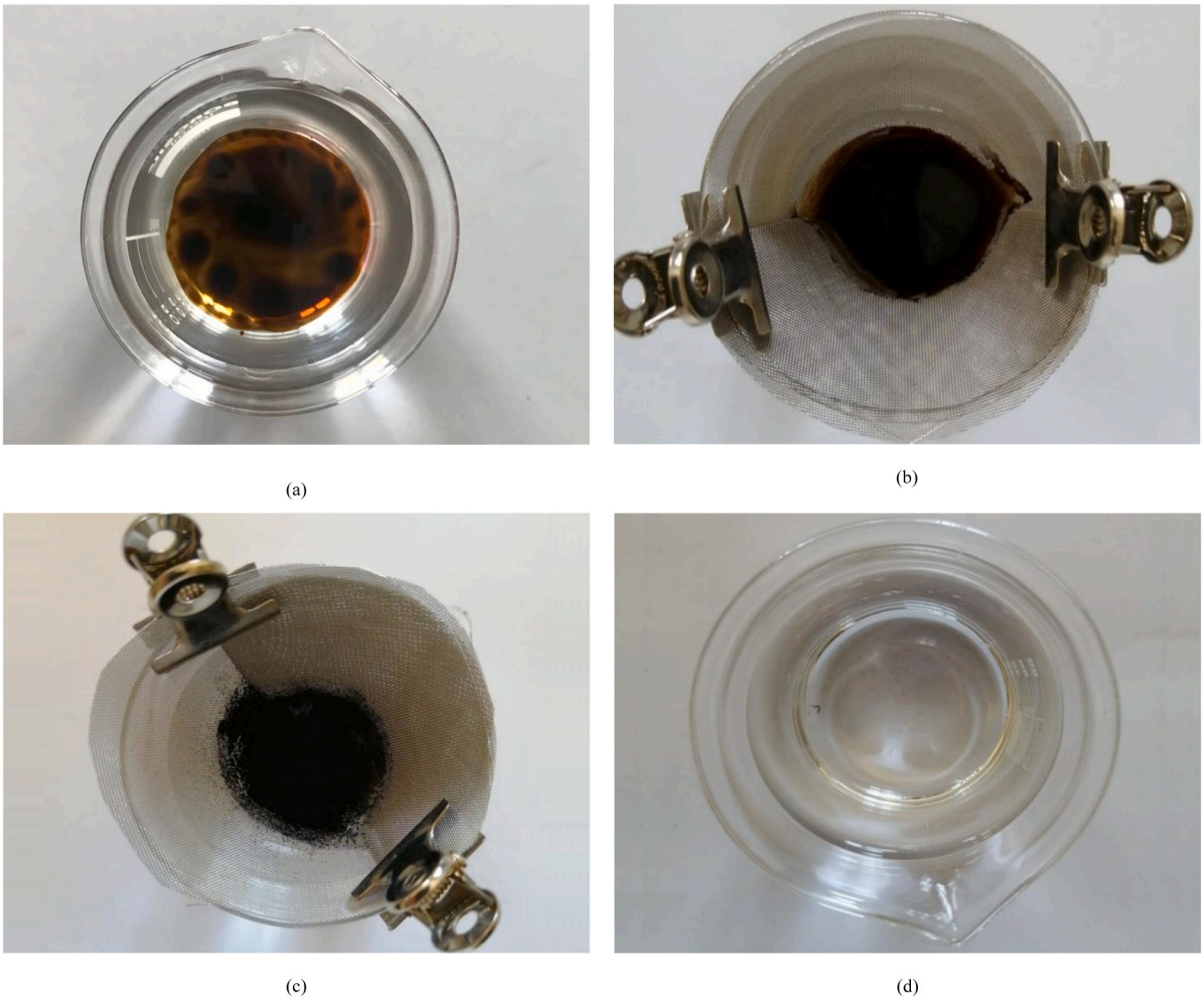

Fig. 2. (a) Oil-water separation (b) light crude oil on water (c) crude oil adsorbed by biocoal (d) oil free water.

cellulose and lignin compounds can be associated with losses during pyrolysis (Gurav et al., 2020).

Torrefied cypress cones were examined for their X-ray diffraction patterns. Since X-ray diffraction is a useful technique for determining the structure and crystallinity of biocoal. The X-ray diffraction pattern of torrefied cypress cones shows two peaks, the most intense one at 2θ equal to 43° being the preferred peak for the amorphous nature of the adsorbent and the second one at 37°. The broad intense peak at 2θ values of 20° can be associated with the presence of a crystal structure in the torrefied cypress cone sample (Li et al., 2016). The peak occurring at 36° is related to the presence of the widely known calcite content. In contrast, the torrefied cypress cones showed an enhanced peak at about 43°, which is associated with the plane of crystalline carbon, indicating the preference of graphite-like structures (Zazycki et al., 2018).

The graphitic structure of the torrefied cypress cone samples was verified using Raman spectra observed at $\lambda_0 = 532$ nm (Bello et al., 2016). The Raman spectrum results show two broad and highly overlapping peaks at 1370 cm^{-1} and 1590 cm^{-1}, indicating disordered graphitic structures (D band) and ordered graphitic structures (G band), respectively (Liu et al., 2014). The D-band is generally attributed to the presence of amorphous (i.e., non-graphitic) structures of the carbonaceous materials such as rings or oxygen-containing groups along with defects, while the G-band indicates the in-plane vibrations of the ordered graphitic sp^2 hybrid carbon atoms, which have been associated with the degree of graphitization (Xie et al., 2016; Zhang et al., 2014). The capacity of sp^3 orbitals indicates the availability of carbon atoms with hydrogen and oxygen bonds, indicating the amorphous nature of the carbonaceous material (Chen et al., 2018). The intensity of the G and D bands demonstrates that the cypress cone- derived biocoal material has a mixture of carbon structures including sp^2 and sp^3 hybridization (Yu et al., 2019). The degree of structural disorder of the carbonaceous materials is usually determined by the intensity ratio of the D band to the G band (I_D/I_G). I_D and I_G represent the maximum intensity (band height) of the D band and the maximum intensity of the G band, respectively (Guizani et al., 2017). This intensity ratio (I_D/I_G) can be used to evaluate the degree of disorder and defects in the biocoal (Bai et al., 2021). I_D/I_G of the roasted cypress cones is 0.94. The intensity ratio of the D/G bands indicates that the pyrolysis process has a smaller detrimental effect on the degree of graphitization and structural stability of the material. On the other hand, the Raman spectrum was also investigated by curve fitting with different band combinations. In general, the Raman spectrum consists of first order (1000–1800 cm^{-1}) and second order (2500–3100 cm^{-1}) regions (Nemanich and Solin, 1979). The first-order region is considered with a combination of three discriminating Lorentzian-shaped bands, including G, D1, and D4 at about 1580, 1350, and 1200 cm^{-1}, and a Gaussian-shaped band (D3) at ~1500 cm^{-1}. All these D bands are associated with a disordered crystal structure or the existence of crystal defects. It has been suggested that the D3 band at ~1500 cm^{-1} appears in the spectrum due to the amorphous carbon fraction of the organic molecules (Jawhari et al., 1995). Although Lorentzian line shape is suggested for this band according to Cuesta et al. (1994) and Dippel et al. (Dippel and Heintzenberg, 1999; Dippel et al., 1999), Gaussian line shape is considered as the best fit for this band because of the distribution of amorphous carbon within the defective

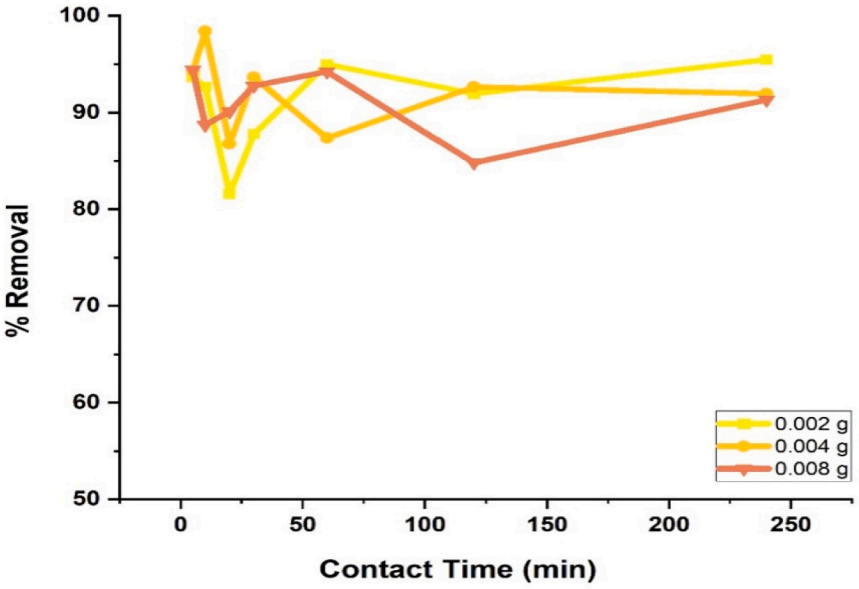

(a)

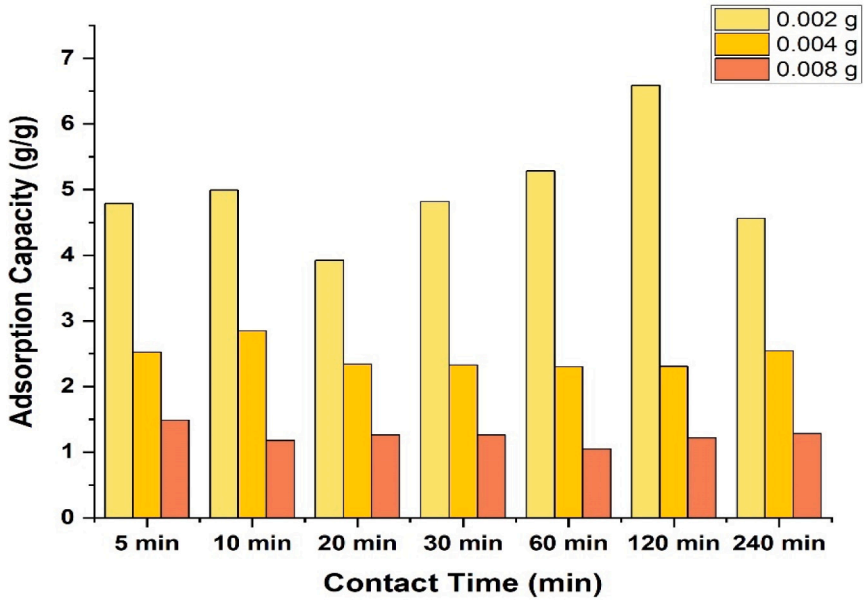

(b)

Fig. 3. Effect of adsorbent dosage: (a) Removal efficiency of crude oil using biocoal adsorbent material (b) Adsorption capacity of light crude oil using biocoal adsorbent material.

graphitic lattice of the char (Jawhari et al., 1995). The spectral analysis of torrefied cypress cones obtained supports the Gaussian line shape. The peak located at ~1350 cm^{-1} corresponds to the D4 band showing C—C and C═C stretching vibrations of polyene-like structures (Dippel and Heintzenberg, 1999; Dippel et al., 1999).

The characteristic surface properties of materials are crucial for describing reactivity. The magnified SEM image of biocoal samples prepared at (300 ± 5.0 °C). SEM image of the biocoal shows that the torrefied cypress cone sample has an amorphous structure. The heterogeneous and amorphous surface of the biocoal is beneficial for the adsorption of crude oil from seawater (Kandanelli et al., 2018; Yan et al., 2020). Moreover, the amorphous structure of the torrefied cypress cone contains pores of different sizes, which are formed by the dehydration and volatilization of the feedstocks during pyrolysis (dos Reis et al., 2021; Tumuluru et al., 2010). These pyrolytic volatiles are cleaved into organic structures of lower molecular weight, which begin to appear on the surface of the biocoal (Thangalazhy-Gopakumar et al., 2010). Due to thermally decomposed polysaccharide residues, carboxyl, hydroxyl, and phenolic groups may form, accumulate, and precipitate on the surface of the biocoal (Tumuluru et al., 2010). This irregular and porous carbonaceous surface of biocoal is beneficial for adsorption of crude oil from seawater (Liou, 2010; Yan et al., 2020).

3.2. Light crude oil adsorption studies

An oil adsorption study was performed using a biocoal adsorbent from torrefaction of cypress cones against light crude oil. 100 mL of seawater from the Bosphorus was added to the beaker and the stainless-steel filter was attached using clamps. Then 0.01 ± 0.005 g of Basra Light Crude Oil was added to the prepared system as shown in Fig. 2.

Fig. 2(a) is used to show the crude oil-water separation in the experimental setup. Fig. 2(b) and (d) show the pre- and post-treatment in the removal of crude oil in water. In this study, specific amounts (0.002, 0.004, and 0.008 g) of biocoal were sprinkled on the water-oil interface after the stainless-steel filter was attached, and then the oil sample was added and incubated at 20 °C for predetermined contact time intervals in all crude oil adsorption batch studies (5, 10, 20, 30, 60, 120, 240 min). After incubation, the stainless-steel filter was removed from the beaker to collect the adsorbent from the seawater surface. These filters, which contained the adsorbent sample along with the adsorbed oil, were dried in an oven at 50° for 1 h to remove the adsorbed water.

The maximum adsorption capacity Q ($g_{oil}/g_{adsorbent}$) and removal efficiency R % for crude oil were calculated using Eqs. (1) and (2):

$$Q(g/g) = \frac{W_f - W_{bc}}{W_{bc}} \quad (1)$$

$$R\% = \frac{W_f - W_{bc}}{W_{io}} \times 100 \quad (2)$$

where W_f is the final weight of biocoal after adsorption (g), W_{bc} is the weight of the pristine cypress cone derived biocoal (g), and W_{io} is the initial weight of light crude oil (g). Adsorbent dosage is an important parameter affecting adsorption efficiency (Elkady et al., 2016).

The effects of adsorbent amount on the percentage of crude oil removal and the adsorption capacity of the biocoal adsorbent were investigated in Fig. 3. It was found that as the adsorbent amount increases, the crude oil removal efficiency shows a decreasing trend until equilibrium is reached within 120 min. Even if the dosage of adsorbent changes, the removal efficiency remains almost at a similar value after 120 min. On the other hand, the percentage of removal increases rapidly in the first 30 min when the dosage of adsorbent is increased. This could be related to the high driving force for mass transfer and the availability of more free binding sites on the adsorbent surface. As time progressed, equilibrium was slowly reached in each dosing experiment due to the saturation of the adsorbent sites with crude oil. Even if sufficient time is waited, it was observed that an increase in the amount of adsorbent leads to a decrease in oil removal efficiency. This can be attributed to the aggregation that occurs due to the higher amount of adsorbent. This aggregation leads to a decrease in the surface area of the adsorbent and thus an increase in the diffusion path length (Elkady et al., 2017).

As the amount of adsorbent increases, the adsorption capacity decreases as the number of unoccupied functional sites increases. Moreover, aggregation, which occurs after a certain time interval, is one of the possible explanations for the decrease in sorption capacity. On the other hand, the oil adsorption capacity from the experiment with an adsorbent dosage of 0.008 g at an adsorption time of 240 min was higher than that from the repeated experiments with a lower adsorbent dosage. This increase in adsorption capacity with increasing adsorbent amount can be attributed to the presence of vacancies for adsorption sites.

3.3. Adsorption kinetic

To better determine the adsorption mechanism with the best fitting kinetic model, different mathematical models were used using the results of the batch adsorption experiments. The kinetic models show the rate of chemical reactions during the adsorption processes and define the reaction pathway and adsorption mechanism for equilibrium access

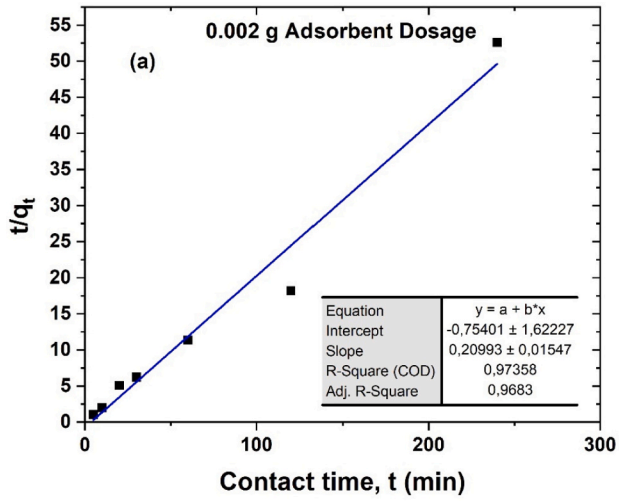

(a)

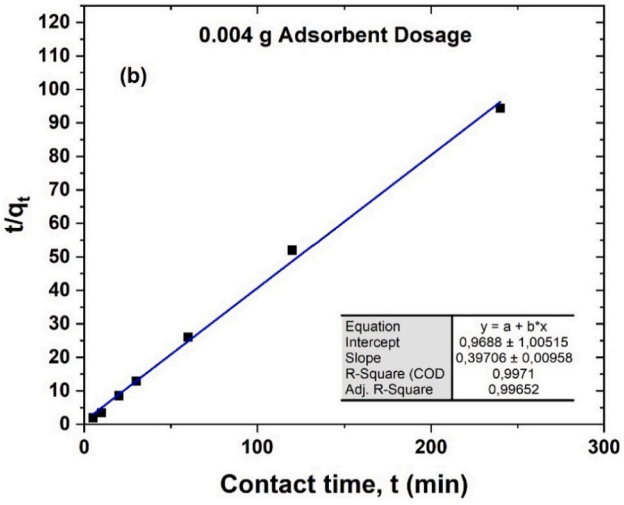

(b)

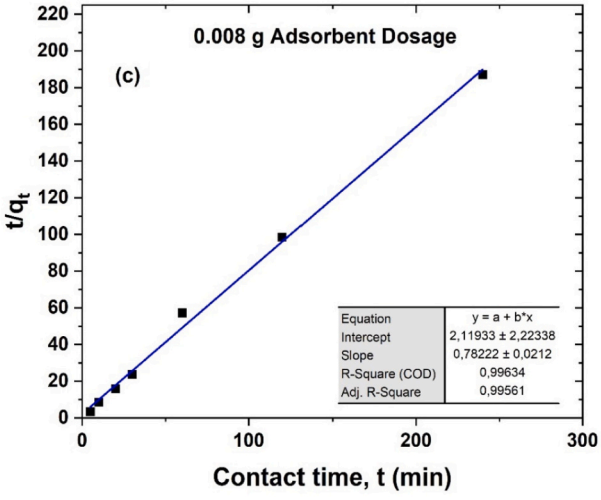

(c)

Fig. 4. Adjustment of experimental results of biocoal adsorbent using the pseudo-second-order model: (a) 0.002 g, (b) 0.004 g, (c) 0.008 g.

Table 1
Pseudo-second-order kinetic model parameters for adsorption of crude oil on torrefied cypress cones.

Adsorbent dosage (g)	Parameters	Value
0.002	$(q_e)_{cal}$ (g/g)	4.7635
	(k_2) (g/g·min)	0.051
	R^2	0.9683
0.004	$(q_e)_{cal}$ (g/g)	2.5185
	(k_2) (g/g·min)	0.1627
	R^2	0.9965
0.008	$(q_e)_{cal}$ (g/g)	1.2784
	(k_2) (g/g·min)	0.2887
	R^2	0.9956

with an acceptable time. The kinetic studies on the adsorption of crude oil on the prepared biocoal adsorbent were carried out using the simulation of the linearized pseudo-second-order model. The agreement of the empirical data with the results of the model was indicated by the correlation coefficient (R^2). The comparatively high R^2 value indicates that the model correctly reproduces the kinetics of crude oil adsorption.

The pseudo-second-order simulation model at pH 7 and 20 °C is expressed by the following kinetic rate statement, which is formulated as follows (Ho and McKay, 1999);

$$\frac{t}{q_t} = \frac{1}{k_2 q_e^2} + \frac{1}{q_e} \times t \tag{3}$$

where t is the contact time (min), q_t is the capacity of the oil (g/g) at time t (min), k_2 is the equilibrium rate constant (l/min) of pseudo-second-order (g/g min), q_e (g/g) is the equilibrium adsorption. As k_2 decreases, the time required to reach equilibrium conditions increases. The main assumption of the adsorption mechanism obeying pseudo-second-order kinetics is that the step limiting the adsorption rate occurs due to the valence forces of the interactions between the adsorbent surface and the oil. The values of k_2 and q_e can be determined from the intercept and slope of the plotted curves made by plotting t/q_t against contact time, t (min) (Fig. 4). When the adsorption process proceeds according to this kinetic model, the plotted curve is a straight line. One of the great advantages of this type of kinetic model is the estimation of q_e parameters with a relatively small experimental error.

The goodness of fit is determined by the R^2 values. The pseudo-second-order kinetic model, as shown in Fig. 4, provided a good fit to all the results of the experiments analyzing the dosage effect because it has a higher coefficient of determination. Therefore, the pseudo-second-order kinetic model is considered representative for the simulation of the adsorption process of petroleum on the biocoal adsorbent, since it has a relatively high coefficient of determination and is valid for almost all contact time variations.

According to the assumption of the pseudo-second-order model, chemisorption is the main adsorption mechanism. On the other hand, the pseudo-second order model based on chemisorption is not suitable for defining the physical adsorption mechanisms (Wang et al., 2020). The chemical adsorption is described by the formation of surface coordination compounds such as interspherical surface complexes between the adsorbate and the surface of the adsorbent. The petroleum nucleates and precipitates on the surface of the adsorbent as a surface precipitate. Another way to determine the adsorption of crude oil on the biocoal adsorbent is to use a partitioning mechanism. The fatty acid groups on the adsorbent have hydrophobic tails that interact with each other and result in non-polar organic structures that help separate the nonionic organic molecules of the crude oil from the water (Banerjee et al., 2006; Sidik et al., 2012). Therefore, it was assumed that the pseudo-first order kinetic model might be insufficient to explain this behavior. In fact, in most published studies on oil spill adsorption, the pseudo-second-order kinetic model was observed to give better results than the pseudo-first-order model (Navarathna et al., 2020; Shokry et al., 2020). The constants obtained from the results of the pseudo-second-order model,

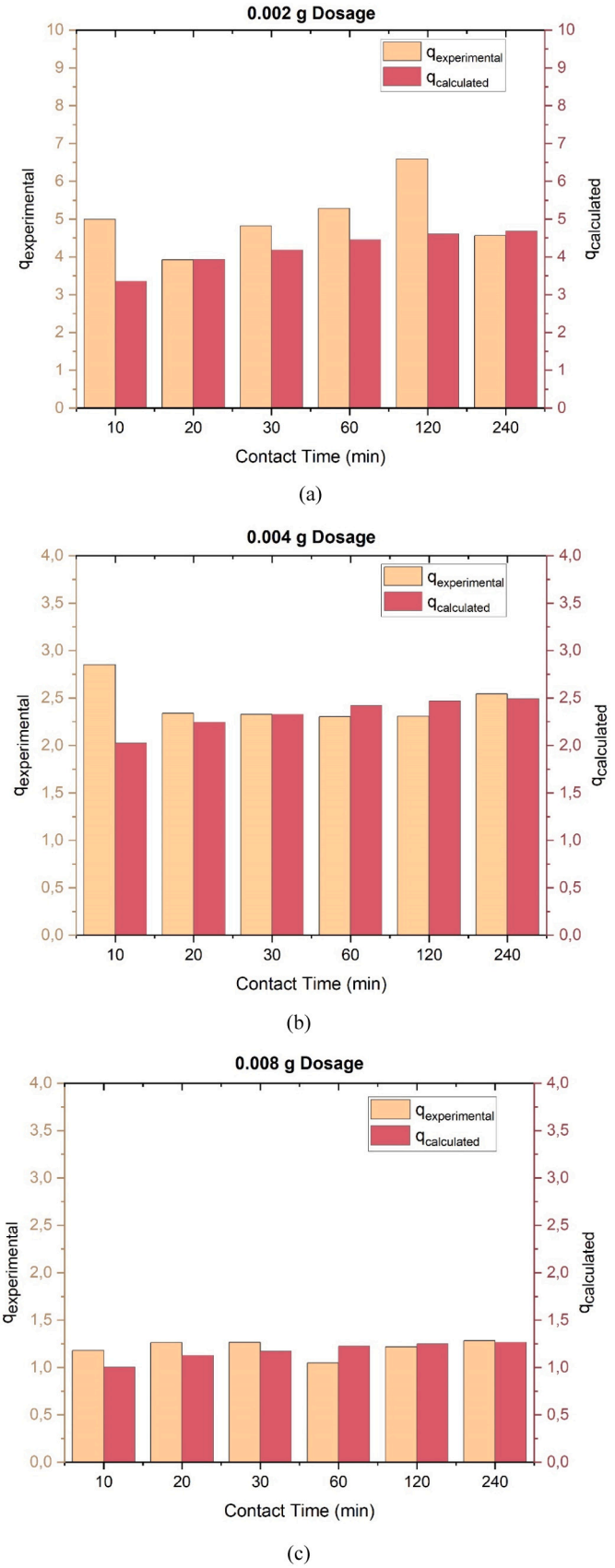

Fig. 5. Comparison of crude petroleum oil adsorption kinetics with experimental results: (a) 0.002 g, (b) 0.004 g, (c) 0.008 g.

including the values for q_e and k_2, were determined based on the slope and intercept, respectively, as indicated in Table 1. The largest R^2 value of 0.9965 was obtained for a dosage of 0.004 g of the biocoal adsorbent sample. The high correlation coefficients indicate that the pseudo-second order adsorption process dominates the adsorption of crude oil on the biocoal adsorbent. A comparison, as seen in Fig. 5, confirms that the kinetic results for adsorption capacity are consistent with the experimentally determined values.

With an initial contact time of 10 min, both the calculated and actual data show that the crude oil is rapidly adsorbed onto the biocoal. It is possible that the presence of free active functional sites on the adsorbent surface is responsible for the initial higher adsorption capacity (Cai et al., 2019; Vyavahare et al., 2019). However, no significant change in adsorption capacity occurred after 10 min because the adsorbent surface was saturated with crude oil (Navarathna et al., 2020).

4. Conclusion

An oil spill is a release of petroleum from its source into the environment that can have long-term and often devastating effects. As a result of this disaster, marine life is threatened worldwide. The use of torrefied cypress cones is an environmentally friendly and cost-effective method that could be used to recover oil from contaminated seawater. In this study, the adsorbent from torrefaction of cypress cones showed remarkable potential for use as an adsorbent in the recovery of light crude oil from seawater with an adsorption capacity of 6.587 g/g and a removal efficiency of 91.94 %.

CRediT authorship contribution statement

Uğur Özveren - Conceptualization.

Berna Kekik, Halime Yakişik and Uğur Özveren - Data Curation (Equal).

Uğur Özveren - Formal Analysis.

Berna Kekik and Uğur Özveren - Investigation.

Berna Kekik, Halime Yakişik and Uğur Özveren - Methodology.

Uğur Özveren - Project Administration.

Uğur Özveren - Resources.

Uğur Özveren - Supervision.

Berna Kekik and Uğur Özveren -Validation (Equal).

Berna Kekik and Uğur Özveren -Visualization (Equal).

Berna Kekik, Halime Yakişik and Uğur Özveren - Writing - (Equal).

Declaration of competing interest

The authors declare that they have no known competing financial interests or personal relationships that could have appeared to influence the work reported in this paper.

Acknowledgment

This work has been supported by Marmara University Scientific Research Projects Coordination Unit under grant number FYL-2021-10275. The authors would like to thank Türkiye Petrol Rafinerileri A.Ş. (TUPRAŞ) for their support.

Appendix A. Supplementary data

Supplementary data to this article can be found online at https://doi.org/10.1016/j.biteb.2022.101139.

References

Bada, B.S., Olarinre, T.A., 2012. Characteristics of soils and heavy metal content of vegetation in oil spill impacted land in Nigeria. In: Proceedings of the Annual International Conference on Soils, Sediments. Water Energy Int., p. 2

Bai, X., Zhang, Y., Shi, J., Xu, L., Wang, Y., Jin, P., 2021. A new application pattern for sludge-derived biochar adsorbent: Ideal persulfate activator for the high-efficiency mineralization of pollutants. J. Hazard. Mater. 419, 126343.

Banerjee, S.S., Joshi, M.V., Jayaram, R.V., 2006. Treatment of oil spill by sorption technique using fatty acid grafted sawdust. Chemosphere 64 (6), 1026–1031.

Belhamdi, B., Merzougui, Z., Laksaci, H., Trari, M., 2019. The removal and adsorption mechanisms of free amino acid l-tryptophan from aqueous solution by biomass-based activated carbon by H3PO4 activation: regeneration study. Phys. Chem. Earth 114, 102791.

Bello, A., Manyala, N., Barzegar, F., Khaleed, A.A., Momodu, D.Y., Dangbegnon, J.K., 2016. Renewable pine cone biomass derived carbon materials for supercapacitor application. RSC Adv. 6 (3), 1800–1809.

Cai, L., Zhang, Y., Zhou, Y., Zhang, X., Ji, L., Song, W., Zhang, H., Liu, J., 2019. Effective adsorption of diesel oil by crab-shell-derived biochar nanomaterials. Materials 12 (2), 236.

Chen, W., Wei, R., Ni, J., Yang, L., Qian, W., Yang, Y., 2018. Sorption of chlorinated hydrocarbons to biochars in aqueous environment: effects of the amorphous carbon structure of biochars and the molecular properties of adsorbates. Chemosphere 210, 753–761.

Chen, J., Zhang, W., Wan, Z., Li, S., Huang, T., Fei, Y., 2019. Oil spills from global tankers: status review and future governance. J. Clean. Prod. 227, 20–32.

Chen, W.-H., Lin, B.-J., Lin, Y.-Y., Chu, Y.-S., Ubando, A.T., Show, P.L., Ong, H.C., Chang, J.-S., Ho, S.-H., Culaba, A.B., 2021. Progress in biomass torrefaction: principles, applications and challenges. Prog. Energy Combust. Sci. 82, 100887.

Cuesta, A., Dhamelincourt, P., Laureyns, J., Martinez-Alonso, A., Tascón, J.D., 1994. Raman microprobe studies on carbon materials. Carbon 32 (8), 1523–1532.

Dippel, B., Heintzenberg, J., 1999. Soot characterization in atmospheric particles from different sources by NIR FT Raman spectroscopy. J. Aerosol Sci. 30, S907–S908.

Dippel, B., Jander, H., Heintzenberg, J., 1999. NIR FT Raman spectroscopic study of flame soot. Phys. Chem. Chem. Phys. 1 (20), 4707–4712.

dos Reis, G.S., Larsson, S.H., Thyrel, M., Pham, T.N., Claudio Lima, E., de Oliveira, H.P., Dotto, G.L., 2021. Preparation and application of efficient biobased carbon adsorbents prepared from spruce bark residues for efficient removal of reactive dyes and colors from synthetic effluents. Coatings 11 (7), 772.

Doshi, B., Sillanpää, M., Kalliola, S., 2018. A review of bio-based materials for oil spill treatment. Water Res. 135, 262–277.

Elkady, M., Hassan, H.S., Hashim, A., 2016. Immobilization of magnetic nanoparticles onto amine-modified nano-silica gel for copper ions remediation. Materials 9 (6), 460.

Elkady, M.F., Hassan, H.S., Amer, W.A., Salama, E., Algarni, H., Shaaban, E.R., 2017. Novel magnetic zinc oxide nanotubes for phenol adsorption: mechanism modeling. Materials 10 (12), 1355.

Gao, Z., Zhang, Y., Song, N., Li, X., 2017. Biomass-derived renewable carbon materials for electrochemical energy storage. Mater. Res. Lett. 5 (2), 69–88.

Goi, A., Kulik, N., Trapido, M., 2006. Combined chemical and biological treatment of oil contaminated soil. Chemosphere 63 (10), 1754–1763.

Guizani, C., Haddad, K., Limousy, L., Jeguirim, M., 2017. New insights on the structural evolution of biomass char upon pyrolysis as revealed by the Raman spectroscopy and elemental analysis. Carbon 119, 519–521.

Gurav, R., Bhatia, S.K., Choi, T.-R., Park, Y.-L., Park, J.Y., Han, Y.-H., Vyavahare, G., Jadhav, J., Song, H.-S., Yang, P., 2020. Treatment of furazolidone contaminated water using banana pseudostem biochar engineered with facile synthesized magnetic nanocomposites. Bioresour. Technol. 297, 122472.

Gurav, R., Bhatia, S.K., Choi, T.-R., Choi, Y.-K., Kim, H.J., Song, H.-S., Lee, S.M., Park, S. L., Lee, H.S., Koh, J., 2021. Application of macroalgal biomass derived biochar and bioelectrochemical system with Shewanella for the adsorptive removal and biodegradation of toxic azo dye. Chemosphere 264, 128539.

Ho, Y.-S., McKay, G., 1999. Pseudo-second order model for sorption processes. Process Biochem. 34 (5), 451–465.

Jawhari, T., Roid, A., Casado, J., 1995. Raman spectroscopic characterization of some commercially available carbon black materials. Carbon 33 (11), 1561–1565.

Kandanelli, R., Meesala, L., Kumar, J., Raju, C.S.K., Peddy, V.R., Gandham, S., Kumar, P., 2018. Cost effective and practically viable oil spillage mitigation: comprehensive study with biochar. Mar. Pollut. Bull. 128, 32–40.

Kartal, F., Özveren, U., 2021. An improved machine learning approach to estimate hemicellulose, cellulose, and lignin in biomass. Carbohydr. Polym. 2, 100148.

Kartal, F., Özveren, U., 2022. Prediction of torrefied biomass properties from raw biomass. Renew. Energy 182, 578–591.

Li, L., Liu, Q., Wang, Y.-X., Zhao, H.-Q., He, C.-S., Yang, H.-Y., Gong, L., Mu, Y., Yu, H.-Q., 2016. Facilitated biological reduction of nitroaromatic compounds by reduced graphene oxide and the role of its surface characteristics. Sci. Rep. 6 (1), 1–10.

Lin, Y.-C., Ho, S.-H., Zhou, Y., Ren, N.-Q., 2018. Highly efficient adsorption of dyes by biochar derived from pigments-extracted macroalgae pyrolyzed at different temperature. Bioresour. Technol. 259, 104–110.

Liou, T.-H., 2010. Development of mesoporous structure and high adsorption capacity of biomass-based activated carbon by phosphoric acid and zinc chloride activation. Chem. Eng. J. 158 (2), 129–142.

Liu, M., Ma, X., Gan, L., Xu, Z., Zhu, D., Chen, L., 2014. A facile synthesis of a novel mesoporous Ge@ C sphere anode with stable and high capacity for lithium ion batteries. J. Mater. Chem. A 2 (40), 17107–17114.

Min, S., Han, J., Shin, E., Park, J., 2004. Improvement of cadmium ion removal by base treatment of juniper fiber. Water Res. 38 (5), 1289–1295.

Navarathna, C.M., Bombuwala Dewage, N., Keeton, C., Pennisson, J., Henderson, R., Lashley, B., Zhang, X., Hassan, E.B., Perez, F., Mohan, D., 2020. Biochar adsorbents with enhanced hydrophobicity for oil spill removal. ACS Appl. Mater. Interfaces 12 (8), 9248–9260.

Nemanich, R.J., Solin, S., 1979. First-and second-order Raman scattering from finite-size crystals of graphite. Phys. Rev. B 20 (2), 392.
Nguyen, T.H., Pham, V.A., Tran, T.T.L., 2016. Research on oil adsorption capacity of carbonized material derived from agricultural by-product (corn cob, corn stalk, rice husk) using in oily wastewater treatment. VNU JS: NST 32 (3).
Nobre, C., Dinis, T., Gonçalves, M., Vilarinho, M., Mendes, B., 2016. Using torrefied biomass wastes as low-cost adsorbents for methylene blue. In: Proceedings of the 3rd International Congress on Water, Waste and Energy Management (EWWM). Rome, Italy, pp. 18–20.
Oliveira, L.M., Oliveira, L.F., Sonsin, A.F., Duarte, J.L., Soletti, J.I., Fonseca, E.J., Ribeiro, L.M., Meili, L., 2020. Ultrafast diesel oil spill removal by fibers from silk-cotton tree: Characterization and sorption potential evaluation. J. Clean. Prod. 263, 121448.
Shokry, H., Elkady, M., Salama, E., 2020. Eco-friendly magnetic activated carbon nano-hybrid for facile oil spills separation. Sci. Rep. 10 (1), 1–17.
Sidik, S., Jalil, A., Triwahyono, S., Adam, S., Satar, M., Hameed, B., 2012. Modified oil palm leaves adsorbent with enhanced hydrophobicity for crude oil removal. Chem. Eng. J. 203, 9–18.
Suhas, P., 2007. Carrott and MML Ribeiro Carrott. Bioresour. Technol. 98 (2301), e2312.
Thangalazhy-Gopakumar, S., Adhikari, S., Ravindran, H., Gupta, R.B., Fasina, O., Tu, M., Fernando, S.D., 2010. Physiochemical properties of bio-oil produced at various temperatures from pine wood using an auger reactor. Bioresour. Technol. 101 (21), 8389–8395.
Tumuluru, J.S., Sokhansanj, S., Wright, C.T., 2010. Biomass Torrefaction Process Review and Moving Bed Torrefaction System Model Development. Idaho National Lab. (INL), Idaho Falls, ID (United States).
Vyavahare, G., Jadhav, P., Jadhav, J., Patil, R., Aware, C., Patil, D., Gophane, A., Yang, Y.-H., Gurav, R., 2019. Strategies for crystal violet dye sorption on biochar derived from mango leaves and evaluation of residual dye toxicity. J. Clean. Prod. 207, 296–305.
Wang, J., Wang, S., 2019. Preparation, modification and environmental application of biochar: a review. J. Clean. Prod. 227, 1002–1022.
Wang, L., Shi, C., Pan, L., Zhang, X., Zou, J.-J., 2020. Rational design, synthesis, adsorption principles and applications of metal oxide adsorbents: a review. Nanoscale 12 (8), 4790–4815.
Xie, L., Sun, G., Su, F., Guo, X., Kong, Q., Li, X., Huang, X., Wan, L., Li, K., Lv, C., 2016. Hierarchical porous carbon microtubes derived from willow catkins for supercapacitor applications. J. Mater. Chem. A 4 (5), 1637–1646.
Yan, L., Liu, Y., Zhang, Y., Liu, S., Wang, C., Chen, W., Liu, C., Chen, Z., Zhang, Y., 2020. ZnCl2 modified biochar derived from aerobic granular sludge for developed microporosity and enhanced adsorption to tetracycline. Bioresour. Technol. 297, 122381.
Yang, H., Yan, R., Chen, H., Lee, D.H., Zheng, C., 2007. Characteristics of hemicellulose, cellulose and lignin pyrolysis. Fuel 86 (12–13), 1781–1788.
Yu, J., Tang, L., Pang, Y., Zeng, G., Wang, J., Deng, Y., Liu, Y., Feng, H., Chen, S., Ren, X., 2019. Magnetic nitrogen-doped sludge-derived biochar catalysts for persulfate activation: internal electron transfer mechanism. Chem. Eng. J. 364, 146–159.
Zazycki, M.A., Godinho, M., Perondi, D., Foletto, E.L., Collazzo, G.C., Dotto, G.L., 2018. New biochar from pecan nutshells as an alternative adsorbent for removing reactive red 141 from aqueous solutions. J. Clean. Prod. 171, 57–65.
Zhang, W., Zhang, H., Xiao, J., Zhao, Z., Yu, M., Li, Z., 2014. Carbon nanotube catalysts for oxidative desulfurization of a model diesel fuel using molecular oxygen. Green Chem. 16 (1), 211–220.